



J. Serb. Chem. Soc. 81 (9) 1069–1079 (2016)
JSCS–4908

Journal of
the Serbian
Chemical Society

JSCS-info@shd.org.rs • www.shd.org.rs/JSCS

UDC 547.75*211:66.094.1.58:549.731.1+
542.913:539.12

Original scientific paper

Synthesis of bis- and tris(indolyl)methanes catalyzed by an inorganic nano-sized catalyst followed by dehydrogenation to hyperconjugated products

ALIREZA KHORSHIDI^{1*}, SHAHAB SHARIATI² and MASOOMEH ABOOTALEBI¹

¹Department of Chemistry, Faculty of Sciences, University of Guilan, P. O. Box 41335-1914, Rasht, Iran and ²Department of Chemistry, Faculty of Sciences, Rasht Branch, Islamic Azad University, Rasht, Iran

(Received 7 February, revised 14 April, accepted 11 May 2016)

Abstract: A set of bis- and tris(indolyl)methanes were prepared and dehydrogenated to their hyperconjugated products in a one-pot fashion. Nano-sized $-\text{SO}_3\text{H}$ functionalized mesoporous KIT-6 coated on magnetite nanoparticles ($\text{Fe}_3\text{O}_4@/\text{SiO}_2@/\text{KIT-6-OSO}_3\text{H}$) was used as an efficient catalyst in the first step of the synthesis, and dehydrogenation was completed using $(\text{NH}_4)_2\text{S}_2\text{O}_8$ after removal of the catalyst. The catalyst was fully characterized by Fourier transform infrared spectroscopy (FT-IR), transmission electron microscopy (TEM) and X-ray powder diffraction (XRD), as well as by its nitrogen adsorption–desorption isotherms. The bis- and tris(indolyl)methanes were studied by UV–Vis spectroscopy before and after dehydrogenation, and effect of the ambient parameters on their spectra was investigated. It was found that bis- and tris(indolyl)methanes have no considerable absorption in the visible range but their partial dehydrogenation due to exposure to air makes them colored. The catalyst, as a new combination of known materials, showed superiority in terms of yield, time, and mild reaction conditions in comparison with those reported previously.

Keywords: magnetite; dehydrogenation; (indolyl)methane; KIT-6; solid acid.

INTRODUCTION

Indole is one of the most visible heterocycles in chemistry and is embodied in a myriad of pharmacologically and biologically active compounds. An outstanding class of these compounds includes bis- and tris(indolyl)methanes, which possess a wide range of biological activities and their synthesis has received considerable interest. A few examples in this context include their application in cancer chemotherapy,¹ dietary supplements for humans,^{2–4} inhibition of bladder

* Corresponding author. E-mail: Khorshidi@guilan.ac.ir
doi:10.2298/JSC160207052K

cancer,⁵ renal cell carcinoma,⁶ and antibacterial, antifungal and anti-inflammatory activities.^{7–9} Generally, bis- and tris(indolyl)methanes are prepared by Friedel–Crafts reaction of indoles with carbonyl compounds in the presence of either protic or Lewis acids; but many other methods have also been reported for their preparation.¹⁰ Most of these contributions, however, have introduced bis- and tris(indolyl)methanes as colored materials.^{11–20} Our involvement in the study of indole-type molecules^{21–23} prompted this study of the chromogenic behavior of bis- and tris(indolyl)methanes, and to determine the key factors in their dehydrogenation using UV–Vis spectroscopy. Moreover, functionalized magnetic core–shell nanoparticles have recently been introduced as efficient catalysts in such transformations.^{24,25} In order to improve the yield and minimize the effect of ambient factors, such as oxygen, moisture and light, on the products, first an efficient heterogeneous catalyst based on nano-sized sulfuric acid functionalized mesoporous KIT-6 coated on magnetite nanoparticles was designed. Magnetite nanoparticles were selected as the core because of their ease of recovery from the reaction mixture by an external magnet and mesoporous KIT-6 was selected as the shell for magnetite nanoparticles because of its well-defined channel system and higher amounts of external hydroxyl groups, ready to be converted to the –SO₃H functionality. Before extension of the mesoporous shell, however, an amorphous silica layer was coated on magnetite nanoparticles to protect them from highly acidic conditions. Subsequently, simple treatment of the core–shell nanocomposite with sulfurochloridic acid in CH₂Cl₂ provided the solid acid catalyst (Fe₃O₄@SiO₂@KIT-6–OSO₃H), which was characterized by FT-IR, TEM, XRD and nitrogen adsorption–desorption isotherms.

EXPERIMENTAL

General

The FT-IR spectra were recorded on a Bruker ALPHA FT-IR spectrometer equipped with an ATR module. ¹H-NMR spectra were obtained on a Bruker DRX-400 Avance spectrometer. Chemical shifts are expressed in ppm downfield from TMS as the internal standard. Melting points were measured on a Büchi Melting Point B-540 instrument and are uncorrected. Elemental analyses were realized using a Carlo-Erba EA1110 CNNO-S analyzer and the obtained values agreed with the calculated ones. X-Ray powder diffraction (XRD) measurements were performed using a Philips diffractometer with monochromatized CuK_α radiation. GC analysis of product mixtures was performed on a GC Chrom from Teif Gostar Faraz Co., Iran (split/splitless injector, CP Sil 8CB column, FID assembly). TEM images were obtained on a Philips MC 10 transmission electron microscope (TEM) with an acceleration voltage of 80 kV. BET measurements were performed on a Sibata surface area apparatus 1100. UV–Vis spectra were recorded on a Shimadzu UV-2501PC spectrometer. Potentiometric titrations were performed on a Metrohm 716 DMS Titrino using a combined glass electrode.

Analytical and spectral data of the synthesized compounds are given in Supplementary material to this paper.

Preparation of Fe₃O₄@SiO₂@KIT-6-OSO₃H nanoparticles

Fe₃O₄ nanoparticles were prepared according to a previous report.²⁶ In order to protect the magnetic core from highly acidic conditions, the Fe₃O₄ nanoparticles were coated with an amorphous silica layer prior to extension of the mesoporous silica KIT-6. To do so, a tetraethyl orthosilicate (TEOS) solution in ethanol (10.8 mL/100 mL) was added dropwise under constant stirring at 80 °C to a dispersion of 1 g Fe₃O₄ nanoparticles in a mixture of ethanol and concentrated ammonia (500 mL/25 mL, 25%). After 2h, the Fe₃O₄@SiO₂ nanoparticles were collected by an external magnet and washed several times with water and ethanol. Mesoporous KIT-6 was coated on Fe₃O₄@SiO₂ nanoparticles according to the literature.²⁷ The -SO₃H functionalization was performed according to a previous report.²⁴

General procedure for the preparation of 2a-k

Indole (2.00 mmol), Fe₃O₄@SiO₂@KIT-6-OSO₃H (50 mg), aldehyde (1.0 mmol) and MeCN (15 mL) were added to a flask and mechanically stirred at room temperature until the disappearance of the starting indole was complete (monitored by TLC). After completion of the first step, the catalyst was removed using an external magnet and a solution of (NH₄)₂S₂O₈ (100 mg) in MeCN (5 mL) was added dropwise over the various periods. After completion of the dehydrogenation step, the mixture was purified by short column chromatography (*n*-hexane/EtOAc, 10:4) to provide the desired products.

Characterization data for products **2g** and **2h** can be found in the Supplementary material to this paper. All of the other products are known compounds and their full characterization data can be found in the literature.^{21,28}

RESULTS AND DISCUSSION

Characterization of the Fe₃O₄@SiO₂@KIT-6-OSO₃H catalyst

In the FT-IR spectrum of Fe₃O₄@SiO₂@KIT-6-OSO₃H (Fig. 1), the band at 600 and the shoulder at 566 cm⁻¹ can be attributed to the Fe-O vibrations of Fe₃O₄ in tetrahedral and octahedral sites, respectively. Asymmetric stretching, symmetric stretching and bending vibrations of Si-O-Si at 1078, 796 and 467 cm⁻¹ were also observed. -SO₃H functionality showed its characteristic bands at 3414, 1224 and 1135 cm⁻¹.²⁴

The wide angle XRD pattern of Fe₃O₄@SiO₂@KIT-6-OSO₃H is shown in Fig. 2 (left), where the peaks at 2θ values of 30.3, 35.7, 43.4, 53.8, 57.3 and 62.9° correspond to Fe₃O₄ nanocrystals (JCPDS No. 19-692).²⁹ The smoothly varying peak at a 2θ value of about 20 results from the amorphous SiO₂ that covers the surface of magnetite nanoparticles when assembling the KIT-6 shell. The XRD patterns for KIT-6 and Fe₃O₄@SiO₂@KIT-6-OSO₃H at small angles are compared in Fig. 2 (right). Three peaks at 2θ 1.0, 1.2 and 1.8° indicate well resolved (211), (220) and (332) planes of mesoporous KIT-6 with *Ia3d* space group. Definitely, the intensities of the XRD peaks decreased and the d spacing was shifted to a smaller angle after coating the mesoporous shell on the magnetite core.

The nitrogen adsorption-desorption isotherm of the Fe₃O₄@SiO₂@KIT-6-OSO₃H nanoparticles showed a characteristic type IV curve (Fig. 3) with a dis-

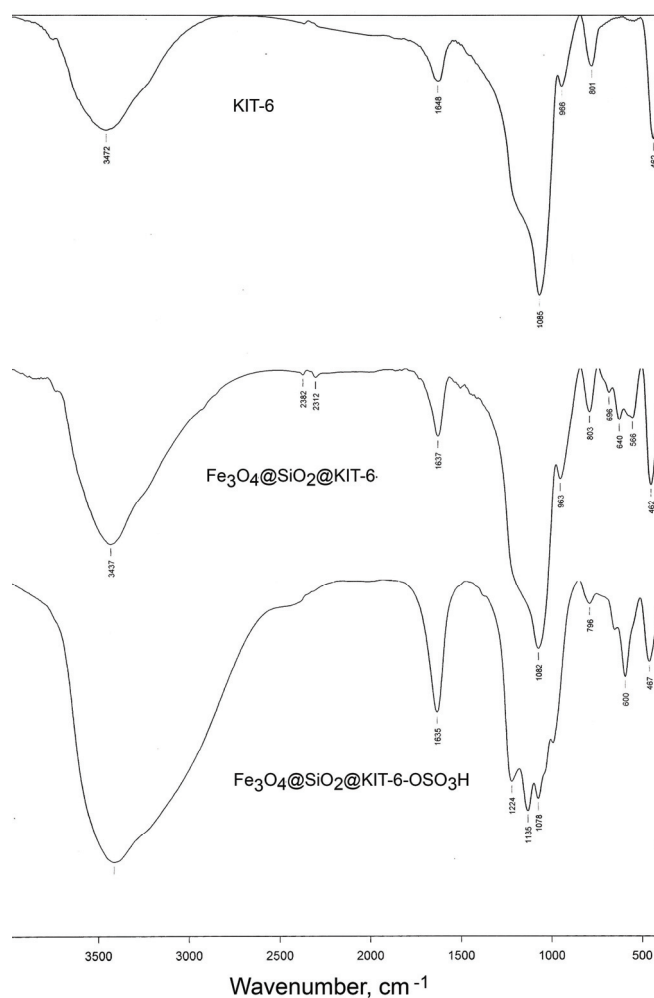


Fig. 1. FT-IR spectrum of KIT-6 (upper), $\text{Fe}_3\text{O}_4@\text{SiO}_2@\text{KIT-6}$ (middle) and $\text{Fe}_3\text{O}_4@\text{SiO}_2@\text{KIT-6-OSO}_3\text{H}$ (lower) nanoparticles.

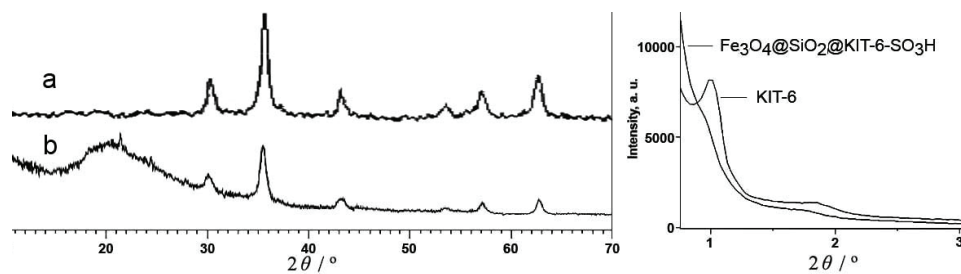


Fig. 2. Left: XRD pattern of a) Fe_3O_4 and b) $\text{Fe}_3\text{O}_4@\text{SiO}_2@\text{KIT-6-OSO}_3\text{H}$; right: XRD patterns for KIT-6 and $\text{Fe}_3\text{O}_4@\text{SiO}_2@\text{KIT-6-OSO}_3\text{H}$ at small angles.

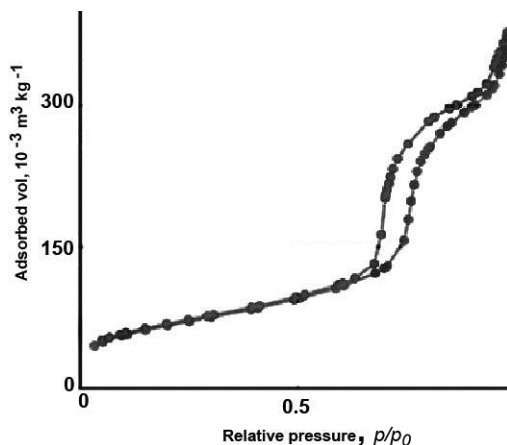


Fig. 3. Nitrogen adsorption–desorption isotherms measured at 77 K for the core–shell structured $\text{Fe}_3\text{O}_4@\text{SiO}_2@\text{KIT-6-SO}_3\text{H}$ nanoparticles.

tinct hysteresis loop in the p/p_0 range of 0.6–0.9, indicating a narrow distribution of mesoporous pore sizes. The corresponding BJH pore size distribution curve also indicated a narrow pore size distribution with a mean pore diameter of about 5 nm. Other textural properties of the $\text{Fe}_3\text{O}_4@\text{SiO}_2@\text{KIT-6-OSO}_3\text{H}$ nanoparticles are as follows: BET surface area: $226.5 \text{ m}^2 \text{ g}^{-1}$, mean pore diameter (BJH): 48 \AA , total pore volume: $0.536 \text{ cm}^3 \text{ g}^{-1}$ and mean pore volume: $0.514 \text{ cm}^3 \text{ g}^{-1}$.

Morphology of the nano-sized particles, however, was demonstrated by transmission electron microscopy (TEM, Fig. 4). $\text{Fe}_3\text{O}_4@\text{SiO}_2@\text{KIT-6-OSO}_3\text{H}$ nanoparticles were observed as many ultrafine agglomerated spherical particles that display dark magnetite cores surrounded by a shell. Particle size distribution analysis showed the mean particle size was about 40 nm.

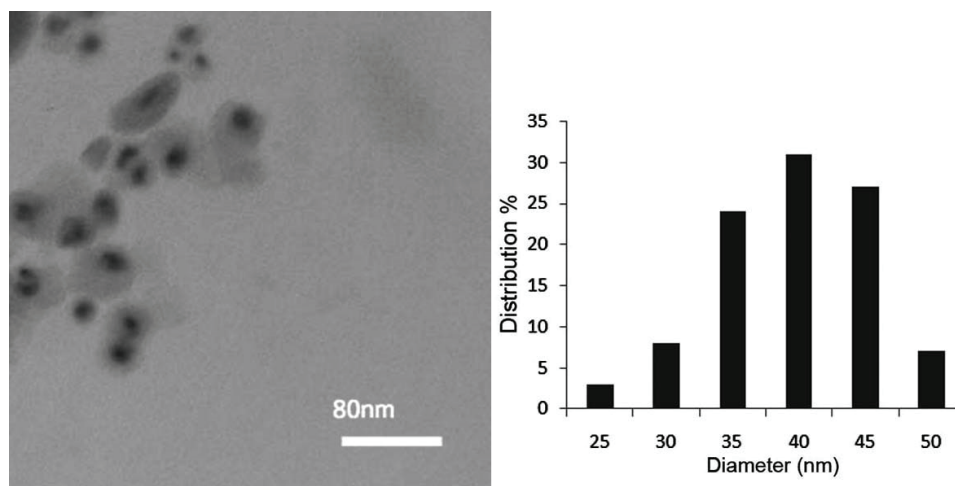
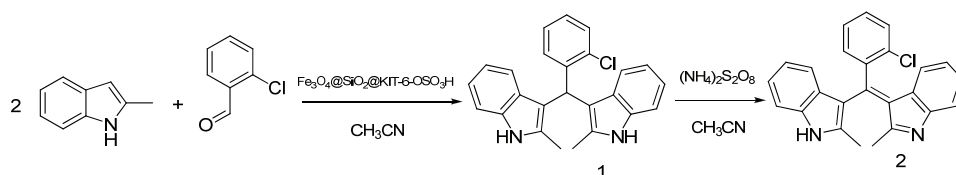


Fig. 4. TEM image of $\text{Fe}_3\text{O}_4@\text{SiO}_2@\text{KIT-6-OSO}_3\text{H}$ nanoparticles (left) and a relevant particle size distribution chart (right).

The quantification of OSO_3H was performed by potentiometric titration of the solution obtained from proton-exchange of a suspension of 100 mg of the catalyst and 25.0 mL of 1.0 M NaCl after stirring overnight.²⁴ The acid content was found to be 2.81 mmol $-\text{SO}_3\text{H}$ per g of the solid acid catalyst.

Synthesis and dehydrogenation of bis- and tris(indolyl)methanes

The characterized catalyst was then used in the one-pot formation and dehydrogenation of bis- and tris(indolyl)methanes to their corresponding hyper-conjugated products. First, 2-chlorobenzaldehyde and 2-methylindole were selected as substrates to determine the optimum reaction conditions with respect to solvent, catalyst loading, temperature and oxidant (Scheme 1).



Scheme 1. One-pot condensation of 2-methylindole and 2-chlorobenzaldehyde followed by dehydrogenation.

Although an excellent yield of 98 % was obtained for the first step in methanol, insolubility of the condensation product in this solvent prevented it from further dehydrogenation (Table I, entry 1).

TABLE I. The effect of experimental parameters on the one-pot Freidel–Crafts condensation reaction of 2-methylindole and 2-chlorobenzaldehyde, and dehydrogenation to the final product; The reaction was performed according to the general experimental procedure

Entry	Catalyst	Loading mg/mmol of aldehyde	T $^{\circ}\text{C}$	Solvent	Oxidant	Yield of 1 %	Yield of 2 %
1	$\text{Fe}_3\text{O}_4@\text{SiO}_2@\text{KIT-6-OSO}_3\text{H}$	50	RT	CH_3OH	$(\text{NH}_4)_2\text{S}_2\text{O}_8$	98	8
2	$\text{Fe}_3\text{O}_4@\text{SiO}_2@\text{KIT-6-OSO}_3\text{H}$	50	RT	CH_3CN	$(\text{NH}_4)_2\text{S}_2\text{O}_8$	92	63
3	$\text{Fe}_3\text{O}_4@\text{MCM-41-OSO}_3\text{H}$	50	RT	CH_3CN	$(\text{NH}_4)_2\text{S}_2\text{O}_8$	84	55
4	$\text{Fe}_3\text{O}_4@\text{MCM-48-OSO}_3\text{H}$	50	RT	CH_3CN	$(\text{NH}_4)_2\text{S}_2\text{O}_8$	87	56
5	$\text{Fe}_3\text{O}_4@\text{SiO}_2@\text{KIT-6-OSO}_3\text{H}$	75	RT	CH_3CN	$(\text{NH}_4)_2\text{S}_2\text{O}_8$	95	64
6	$\text{Fe}_3\text{O}_4@\text{SiO}_2@\text{KIT-6-OSO}_3\text{H}$	50	RT	CH_3CN	Air	92	5
7	$\text{Fe}_3\text{O}_4@\text{SiO}_2@\text{KIT-6-OSO}_3\text{H}$	5	RT	CH_3CN	H_2O_2	65	27
8	KIT-6- OSO_3H	25	RT	CH_3CN	$(\text{NH}_4)_2\text{S}_2\text{O}_8$	90	60
9	$\text{Fe}_3\text{O}_4@\text{SiO}_2@\text{KIT-6-OSO}_3\text{H}$	50	50	CH_3CN	$(\text{NH}_4)_2\text{S}_2\text{O}_8$	87	30

In CH_3CN , however, dehydrogenation was improved. Other $-\text{SO}_3\text{H}$ functionalized core–shell solid acid catalysts, on the other hand, resulted in lower yields (entries 3 and 4). This may be attributed to their lower acid content according to previous reports.^{24,29} The surface silanol groups convertible to acid func-

ionality, in fact, are directly proportional to surface area of the mesoporous shell. Elevated temperature also had an undesirable effect on the yield (entry 9). Molecular oxygen (O_2), although not as effective as $(NH_4)_2S_2O_8$, may be taken into account for the partial oxidation of bis- and tris(indolyl)methanes and coloration of these material during work-up. In order to screen the trend of oxidation, a freshly prepared 1.0×10^{-5} M solution of **1** in CH_3CN was titrated with $(NH_4)_2S_2O_8$, and UV-Vis spectra at different stages were recorded. As shown in Fig. 5, initially, no considerable absorption was observed in the visible range of spectrum and the solution was almost colorless. Upon oxidation however, two new maxima were observed at about 420 and 525 nm, which may be due to the bathochromic shift of the corresponding transitions to the visible region. The same transitions were also observed when the solution was sparged with air for 30 min.

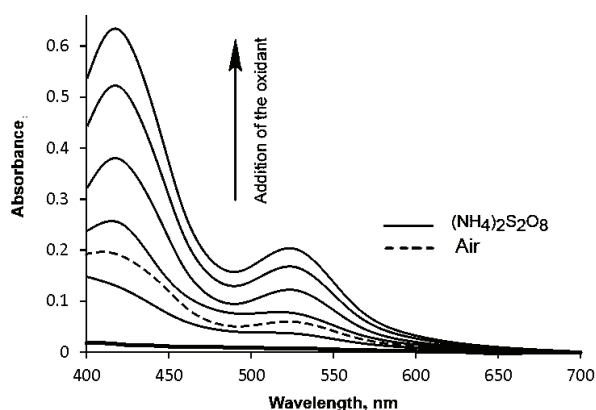


Fig. 5. Titration of a 1.0×10^{-5} M solution of **1** in CH_3CN with $(NH_4)_2S_2O_8$ (solid lines) and the effect of air sparged into the solution for 30 min (dashed line).

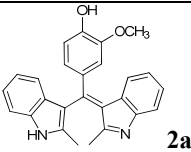
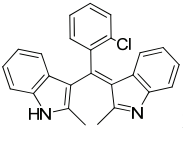
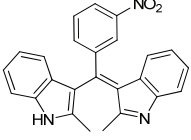
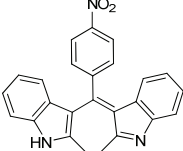
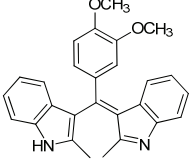
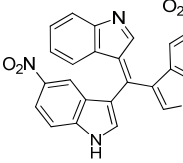
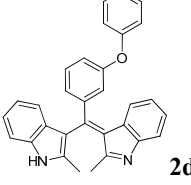
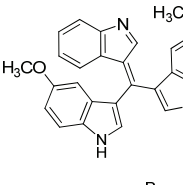
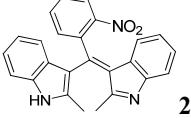
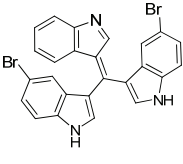
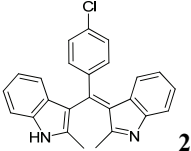
With the optimized conditions to hand, a variety of dehydrogenated products was prepared. Typical results are shown in Table II.

Obviously, a moderate improvement in comparison with a previously reported protocol²¹ was obtained for the dehydrogenated products.

One major advantage of the new catalyst, however, is its recyclability. After completion of the first step (monitored by GC), the catalyst was removed by an external magnet and the oxidant was added to accomplish dehydrogenation. The recovered catalyst was used in successive runs for the first step in the reaction of 2-chlorobenzaldehyde and 2-methylindole. The yields of the corresponding bis-(indolyl)methane were 97, 97, 97, 95, 93, 88 and 80 %, respectively. This result shows that the catalyst maintains its activity at least for six runs with no considerable loss of activity, which promises minimization of the waste. Although decrease in the efficiency of the catalyst invokes a possible leaching of the acid

functionality into the solution, the catalyst recovered after the 6th run was found to have the same acid content (2.80 mmol g⁻¹).

TABLE II. Dehydrogenated bis- and tris(indolyl)methanes obtained *via* Fe₃O₄@SiO₂@KIT-6-OSO₃H nanoparticles catalyzed condensation of indoles and aldehydes, and subsequent dehydrogenation by (NH₄)₂S₂O₈ in CH₃CN under mild conditions

Product ^a	Time ^b , min	Yield ^c , %	Product ^a	Time ^b , min	Yield ^c , %
 2a	3, 150	77	 2g	5, 130	70
 2b	5, 120	68	 2h	5, 160	75
 2c	5, 120	65	 2i	5, 120	54
 2d	5, 150	70	 2j	3, 100	65
 2e	7, 210	70	 2k	5, 45	58
 2f	5, 120	75			

^aProducts were prepared according to general experimental procedure and identified in comparison with authentic samples; ^breaction time of the first step (condensation) and the second step (dehydrogenation); ^cisolated yield

Chromogenic and sensing behavior of the dehydrogenated bis(indolyl)methanes

Starting with 4-nitrobenzaldehyde, the chromogenic and sensing behavior of the bis(indolyl)methane, **1h**, and its dehydrogenated product, **2h**, against various

anions were studied. As shown in Fig. 6 (left), while **1h** had no significant absorption in the visible range, **2h** shows two maxima at about 410 and 540 nm, which may be attributed to $n \rightarrow \pi^*$ transitions from the :N and :NH functionalities of the two indole ring systems. In both cases, the absorption bands of **1h** and **2h** were red-shifted after selective interaction with CN^- . In the case of **2h**, the observed spectral change was in accord with further dehydrogenation of **2h** by CN^- in solution, which results in decrease in the intensity of the 540 nm band and an increase in the 410 nm band, with a simultaneous bathochromic shift of both to new positions (590 and 450 nm, respectively). The most intense color change against anions, however, was observed for **1h** from colorless to yellow in the presence of 1 eq of CN^- . This promises **1h** as a selective colorimetric chemosensor for selective sensing of CN^- in solution (Fig. 6, right).

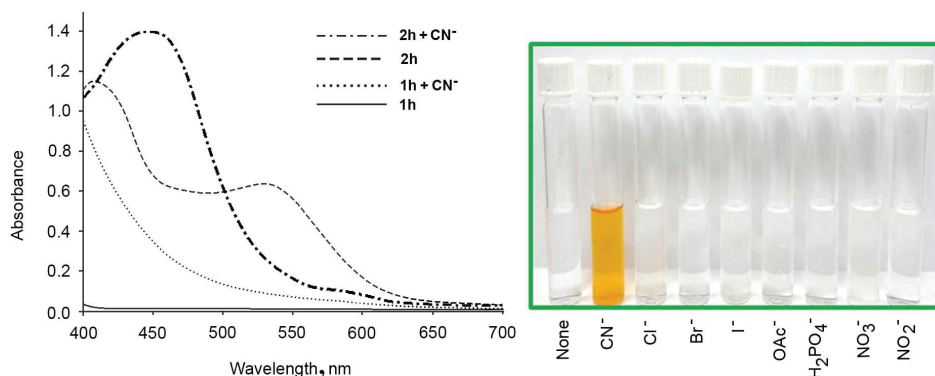


Fig. 6. Spectral changes of **1h** and **2h** (2.5×10^{-5} M in CH_3CN) against 1 eq. of CN^- (left) and the selective response of **1h** to CN^- (right).

Changing the substituents of the phenyl ring in a dehydrogenated product affected its spectrum in the visible region as illustrated in Fig. 7. As expected, the positions of the bands were related to the electron-releasing or -withdrawing nature of the functional groups and their position on the ring. Generally, a more

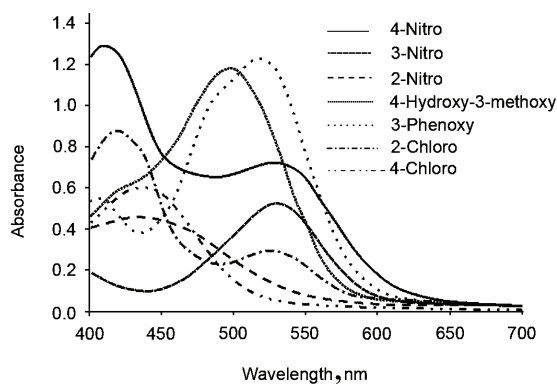


Fig. 7. Spectral changes of the dehydrogenated bis(indolyl)-methanes against various substituents on the phenyl ring.

electron-withdrawing substituent, especially at the *para*- position, resulted in a greater bathochromic shift of the maxima.

CONCLUSIONS

In conclusion, a recyclable catalyst for one-pot preparation and dehydrogenation of bis- and tris(indolyl)methanes under very mild conditions has been prepared. The new synthetic protocol improved the yield of such products. Other advantages of the present protocol include ease of catalyst recycling, ease of work-up and minimization of waste. It was also shown that bis- or tris(indolyl)methanes by virtue of their non-conjugated structure are not inherently colored and that partial oxidation by air during work-up is responsible for their color.

SUPPLEMENTARY MATERIAL

Characterization data for the synthesized compounds are available electronically at the pages of journal website: <http://www.shd.org.rs/JSCS/>, or from the corresponding author on request.

Acknowledgements. Partial support of this study by the Research Council of the University of Guilan is gratefully acknowledged.

ИЗВОД

СИНТЕЗА БИС- И ТРИС(ИНДОЛИЛ)МЕТАНА КАТАЛИЗОВАНА НЕОРГАНСКИМ НАНОКАТАЛИЗАТОРОМ УЗ НАКНАДНУ ДЕХИДРОГЕНИЗАЦИЈУ ДО ХИПЕРКОНЈУГОВАНИХ ПРОИЗВОДА

ALIREZA KHORSHIDI¹, SHAHAB SHARIATI² и MASOOMEN ABOOTALEBI¹

¹Department of Chemistry, Faculty of Sciences, University of Guilan, P. O. Box 41335-1914, Rasht, Iran u

²Department of Chemistry, Faculty of Sciences, Rasht Branch, Islamic Azad University, Rasht, Iran

Серија бис- и трис(индолил)метана је синтетисана и дехидрогенизована до хиперконјугованих производа. У првој фази синтезе, као ефикасан катализатор, коришћен је наночестични магнетит са превлаком мезопорозног $-\text{SO}_3\text{H}$ функционализованог KIT-6 ($\text{Fe}_3\text{O}_4@\text{SiO}_2@\text{KIT}-6-\text{OSO}_3\text{H}$). Дехидрогенизација је изведена коришћењем $(\text{NH}_4)_2\text{S}_2\text{O}_8$, након уклањања катализатора. Катализатор је окарактерисан применом инфрацрвене спектроскопије са Фуријеовим трансформацијама (FTIR), трансмисионом електронском микроскопијом (ТЕМ) и рендгенском дифракционом анализом (XRD), као и адсорпцијом азота на температури течног азота. Узорци бис- и трис(индолил)метана су анализирани UV-Vis спектроскопијом пре и након дехидрогенизације и испитан је утицај амбијенталних параметара на њихове спектре. Показано је да бис- и трис(индолил)метани немају значајну апсорпцију у видљивом делу спектра, па је њихова обојеност резултат парцијалне дехидрогенизације због изложености ваздуху. Узимајући у обзир принос реакције и време реакције, као и благе реакционе услове, синтетисани катализатор, као нова комбинација познатих материјала, показао је супериорност у поређењу са раније публикованим резултатима.

(Примљено 7. фебруара, ревидирано 14. априла, прихваћено 11. маја 2016)

REFERENCES

1. S. Safe, S. Papineni, S. Chintharlapalli, *Cancer Lett.* **269** (2008) 326

2. C. Bonnesen, I. M. Eggleston, J. D. Hayes, *Cancer Res.* **61** (2001) 6120
3. M. J. Anderton, M. M. Manson, R. Verschoyle, A. Gescher, W. P. Steward, M. L. Williams, D. E. Mager, *Drug Metab. Dispos.* **32** (2004) 632
4. T. H. Carter, K. Liu, W. Ralph, D. Chen, M. Qi, S. Fan, F. Yuan, E. M. Rosen, K. J. Auburn, *J. Nutr.* **132** (2002) 3314
5. T. Inamoto, S. Papineni, S. Chintharlapalli, S. D. Cho, S. Safe, A. M. Kamat, *Mol. Cancer Ther.* **7** (2008) 3825
6. M. York, M. Abdelrahim, S. Chintharlapalli, S. D. Lucero, S. Safe, *Clin. Cancer Res.* **13** (2007) 6743
7. G. Sivaprasad, P. T. Perumal, V. R. Prabavathy, N. Mathivanan, *Bioorg. Med. Chem. Lett.* **16** (2006) 6302
8. A. Kamal, M. N. A. Khan, K. S. Reddy, Y. Srikanth, S. K. Ahmed, K. P. Kumar, U. S. N. Murthy, *J. Enzyme Inhib. Med. Chem.* **24** (2009) 559
9. K. Sujatha, P. T. Perumal, D. Muralidharan, M. Rajendran, *Indian J. Chem., B* **48** (2009) 267
10. M. Shiri, M. A. Zolfigol, H. G. Kruger, Z. Tanbakouchian, *Chem. Rev.* **110** (2009) 2250
11. H. Veisi, B. Maleki, F. H. Eshbala, H. Veisi, R. Masti, S. S. Ashrafi, M. Baghayeri, *RSC Adv.* **4** (2014) 30683
12. A. Kundu, A. Ganguly, K. Dhara, P. Patra, N. Guchhait, *RSC Adv.* **5** (2015) 53220
13. E. Oliveira, R. M. Baptista, S. P. Costa, M. M. M. Raposo, C. Lodeiro, *Photochem. Photobiol. Sci.* **13** (2014) 492
14. S. A. Mulla, A. Sudalai, M. Y. Pathan, S. A. Siddique, S. M. Inamdar, S. S. Chavan, R. S. Reddy, *RSC Adv.* **2** (2012) 3525
15. G. S. Kumar, S. Kumaresan, A. A. M. Prabhu, N. Bhuvanesh, P. Seethalakshmi, *Spectrochim. Acta, A* **101** (2013) 254
16. M. A. Zolfigol, P. Salehi, M. Shiri, Z. Tanbakouchian, *Catal. Commun.* **8** (2007) 173
17. S. Khaksar, A. Rouhollahpour, S. M. Talesh, *J. Fluorine Chem.* **141** (2012) 11
18. S. J. Ji, S. Y. Wang, Y. Zhang, T. P. Loh, *Tetrahedron* **60** (2004) 2051
19. M. Rekha, H. Manjunath, N. Nagaraju, *J. Ind. Eng. Chem.* **19** (2013) 337
20. A. K. Chakraborti, S. R. Roy, D. Kumar, P. Chopra, *Green Chem.* **10** (2008) 1111
21. A. Khorshidi, N. Mardazad, Z. Shaabanzadeh, *Tetrahedron Lett.* **55** (2014) 3873
22. A. Khorshidi, K. Tabatabaeian, *J. Mol. Catal., A: Chem.* **344** (2011) 128
23. A. Khorshidi, *Chin. Chem. Lett.* **23** (2012) 903
24. A. Khorshidi, S. Shariati, *RSC Adv.* **4** (2014) 41469
25. A. Khorshidi, S. Shariati, *Chin. J. Catal.* **36** (2015) 778
26. A. Khorshidi, S. Shariati, P. Rahimi, *Arabian J. Chem.* (2015) in press, doi: 10.1016/j.arabjc.2015.04.002
27. F. Kleitz, S. H. Choi, R. Ryoo, *Chem. Commun.* (2003) 2136
28. K. Tabatabaeian, M. Mamaghani, N. O. Mahmoodi, A. Khorshidi, *Can. J. Chem.* **84** (2006) 1541
29. J. H. Jang, H. B. Lim, *Microchem. J.* **94** (2010) 148.